Nanostructured materials for photon detection

Gerasimos Konstantatos[1,2] and Edward H. Sargent[1]*

The detection of photons underpins imaging, spectroscopy, fibre-optic communications and time-gated distance measurements. Nanostructured materials are attractive for detection applications because they can be integrated with conventional silicon electronics and flexible, large-area substrates, and can be processed from the solution phase using established techniques such as spin casting, spray coating and layer-by-layer deposition. In addition, their performance has improved rapidly in recent years. Here we review progress in light sensing using nanostructured materials, focusing on solution-processed materials such as colloidal quantum dots and metal nanoparticles. These devices exhibit phenomena such as absorption of ultraviolet light, plasmonic enhancement of absorption, size-based spectral tuning, multiexciton generation, and charge carrier storage in surface and interface traps.

The visible light that we are all used to seeing and recording represents just a small fraction of the information that radiation carries about our world. For example, X-rays enable imaging in medicine and inspection of civil infrastructure; high-resolution ultraviolet metrology resolves lithographically defined semiconductors[1] and living cells[2]; and infrared sensing underpins night vision[3] and atmospheric spectroscopy for gas detection[4].

Detectors made from crystalline silicon are routinely used for imaging applications at visible and near-infrared wavelengths, and the advent of Complementary Metal Oxide Semiconductor (CMOS) image sensors[5] has led to a multibillion-dollar annual market for digital cameras and other image sensors[6]. The compatibility of silicon photodiodes with silicon electronics enables light sensing, low-noise electronic read out, multiplexing and even digital image processing on a single chip[7].

However, this powerful technology is not without its limitations. Crystalline silicon can absorb wavelengths only below 1.1 μm, which means that it fails to absorb most of the infrared spectrum. In addition, its absorption remains weak over the entire spectrum, only exceeding 10^4 cm^{-1} at 500 nm (which is blue light)[8]. Long interaction lengths and optical crosstalk reduction strategies are needed to achieve high sensitivity at near-infrared and red wavelengths, especially as pixels are increasingly miniaturized. Furthermore, the high mobility and long lifetime for electron–hole pairs in silicon — which are usually considered to be advantages in electronics — lead to photocarrier diffusion[9], which can cause crosstalk and blurring of optical signals between neighbouring pixels. At the ultraviolet wavelengths relevant to machine vision and the diagnosis of skin cancer, the ultrashort absorption lengths found in silicon lead to the generation of electron–hole pairs close to highly recombinative surfaces states, curtailing ultraviolet sensitivity in standard devices and requiring specialized processing[10].

Materials that can absorb light where silicon cannot are therefore of great practical interest. So, too, are avenues to enhance photodetector sensitivity in all spectral regimes, including the visible. Strategies include top-surface detectors having 100% fill factor, and signal amplification within the photodetector itself, including carrier multiplication and photoconductive gain[11,12]. There is thus an intense interest in new materials and structures that expand the spectrum of absorption, minimize the thickness of semiconductor needed to absorb light completely, and amplify the signal. Ideally, these materials should be compatible for integration with

silicon electronics[13], or with flexible substrates such as those based on organic and polymer materials[14]. Ink-jet printing, solution casting, low-temperature evaporation, and layer-by-layer techniques are therefore very attractive alternatives to high-temperature epitaxy[15].

Here we review recent advances in light sensing, focusing on materials that are compatible with low-temperature processing and large-area integration. These include colloidal quantum dots (CQDs)[16] and metal nanoparticles[17], in which nanoscale phenomena such as quantum confinement[18] and plasmonic effects[19] play a principal role. Excellent and up-to-date reviews exist in the related area of epitaxially-grown nanostructured materials and the devices made from them[20].

CQDs are an example of nanostructured materials that can be synthesized and processed from the solution phase. They benefit from the quantum size effect, wherein the bandgap of the material is strongly dependent on the size of the nanocrystals. Rapid advances in CQD synthesis and photophysics[18] have led to a high degree of control over nanoparticle size, shape and composition[16]. The confinement of charge carriers in a CQD means that they occupy discrete energy levels, similar to the electrons in an atom. The strong confinement experienced by the charge carriers also influences the various mechanisms that are involved in charge transport in solids made from quantum dots, including delocalization[21], variable-range hopping[22], slow carrier relaxation[23], and the interactions between electrons and holes[24–28]. Multicarrier effects in nanoparticles can be exploited in photodetection applications to achieve performance enhancements through carrier multiplication. More broadly, these effects can provide optical gain for lasing, strong nonlinear interactions for optical signal processing, and the possibility of enhanced light harvesting in photovoltaics.

In this review we discuss two different types of photodetector (photodiodes and photoconductors); summarize the performance of solution-processed photodetectors; discuss the device concepts, materials and physical phenomena that have underpinned these improvements in performance; discuss the use of plasmonic effects to achieve performance enhancements through the concentration of light; and present other advanced photodetector concepts.

Quantitative progress in performance

Table 1 summarizes the figures of merit used to characterize photodetectors, and Table 2 summarizes progress in these figures of merit for solution-processed devices[29–45]. Reports in which sensitivity

[1]Department of Electrical and Computer Engineering, University of Toronto, 10 King's College Road, Toronto, Ontario M5S 3G4, Canada, [2]Present address: ICFO-Institut de Ciencies Fotoniques, Mediterranean Technology Park, 08860 Castelldefels, Barcelona, Spain.*e-mail: ted.sargent@utoronto.ca

Table 1 | Photodetector definitions and figures of merit.

Quantity	Symbol/acronym	Unit	Definition
Responsivity	R	A W^{-1}	Photocurrent flowing in a detector divided by incident optical power
Dark current Dark-current density	I_d J_d	A A cm^{-2}	Current (density) flowing in the absence of illumination. In an unbiased
Quantum efficiency External quantum efficiency	QE EQE	%	In a photodiode, the ratio of photocurrent (in electrons per second) to photon fluence incident on the device (photons per second). Related to responsivity via the photon energy: $R = QE/E_{photon}$ (where E_{photon} is measured in electronvolts). In a photoconductor, the term QE is sometimes used synonymously with absorbance.
Internal gain	G_{int}	Unitless	In a photoconductor, the ratio of photocurrent (in electrons per second) to photon absorbed.
External gain	G_{ext}	Unitless	In a photoconductor, the ratio of photocurrent (in electrons per second) to photon incident. $G_{ext} = QE \times G_{int}$
Noise current	I_{noise}	$A/\sqrt{Hz}$	The random root mean square fluctuation in current when bandwidth is limited to 1 Hz.
Noise-equivalent power	NEP	$W/\sqrt{Hz}$	The minimum detectable power, that is, the optical signal in watts at which the electrical signal-to-noise ratio in the detector is equal to unity (0 dB), when bandwidth is limited to 1 Hz.
Normalized detectivity	D^*	$cm\sqrt{Hz}/W$ (Jones)	A measure of detector sensitivity that enables comparison even when detector area A and bandwidth B are different. $D^* = (\sqrt{AB})/NEP$.

is given, as well as those from which it can be inferred, are both included in Table 2.

The results in Table 2 fall into two performance classes, one corresponding to photodiodes and the other to photoconductors. In a photodiode, the electrons and holes generated by the incoming photons move to opposite electrical contacts (Fig. 1a), so the quantum efficiency of such devices cannot be higher than one (unless effects such as avalanche or carrier multiplication are exploited). However, photodiodes can have fast response times — shorter than electron–hole recombination times — which are typically microseconds or less for the direct-gap semiconductors commonly used. Photodiodes thus populate the higher-frequency reaches of Table 2.

Photoconductors, on the other hand, are capable of high gain[46] because one type of charge carrier (say, holes) is able to circulate through an external circuit many times before it recombines with its opposite carrier (say, electrons), which meanwhile remain trapped in the photoconductor bulk (Fig. 1b). Table 2 lists a number of photoconductors with responsivity values in the range of 100–1,000 A W^{-1}, corresponding to gains of 100–1,000. Although these high gains increase responsivity and simplify the job of any photodetector read-out circuits, they also reduce the bandwidth because of the long circulating carrier lifetimes involved.

The performance of a photodetector can be improved, not only by maximizing its electrical response to light, but also by minimizing the noise in its electrical output, which can obscure real signals. One way to compare detector sensitivities is therefore to examine the signal-to-noise level at a given illumination intensity. Or, conversely, one can examine the noise-equivalent power, which reports the optical power at which the signal-to-noise ratio (SNR) is one (or 0 dB). This noise level is very low, corresponding in some photodetectors to single-photon detection per integration period[47].

The detectivity D^* (formally defined in Table 1, and measured in units called Jones) seeks to normalize for variations in device area and speed of response, thus providing a figure of merit that enables comparison among different devices[48]. Table 2 shows that the best solution-processed detectors have achieved D^* values of up to 5×10^{13},

which is comparable to the best values reported for single-crystal photodiodes. This a remarkable achievement because single-crystal photodiodes have benefited from several decades of engineering, including both materials purification and device structure optimization, whereas solution-processed detectors have reached similar levels of performance after just three years of development.

Photodiode mechanisms and performance

Photodiodes rely on the use of two media — at least one of them being a semiconductor — in which a significant difference in the materials' work functions produces a built-in potential. An internal field in the semiconductor depletion region near the junction propels electrons and holes in opposite directions. In the simple case of a fully depleted device, high internal quantum efficiency is achieved if $t_{life} > t_{extract}$, where t_{life} is the lifetime of excess charge carriers, and $t_{extract} = L^2/\mu V_{bi}$ is the time taken to transport them to their respective contacts through the built-in field (L is the contact separation, μ is the mobility of the slower carrier and V_{bi} is the built-in potential across the junction[49].

In conventional crystalline semiconductors, mobilities lie in the range of 10^2 cm^2 V s^{-1} and above: charge carriers are thus readily swept a distance of 1 μm through a built-in potential of 1 V in times faster than nanoseconds. This comfortably outpaces the recombination time in both direct and indirect semiconductors. Solution-processed semiconductors have much lower mobilities — 10^{-5}–10^{-3} cm^2 V s^{-1} are typical — therefore, even for a thin depletion region 100 nm thick and a typical built-in voltage of 1 V, drift times are in the range of 100 ns–10 μs. Fortunately, some of the most promising semiconductors incorporated into CQDs used to produce solution-processed photodetectors (Fig. 1d) have unusually long exciton lifetimes — greater than 1 μs (ref. 50) — which have led to excellent photodiode quantum efficiencies, with even the first reports well above 50% when absorbance was high[49,51–56]. The high internal quantum efficiencies that these findings entail also indicate that — when their surfaces are well passivated using suitably functionalized ligands — CQD solids achieve carrier lifetimes

Table 2 | Progress in solution-processed photodetector performance.

Ref.	Year	λ (nm)	EQE (%)/Responsivity (A W⁻¹)	D* measured (Jones)*	D* inferred (Jones)†	3 dB BW (Hz)	Mechanism	Material	Features
29	1994	400–650	0.2 A W^{-1}		3×10^{10}	10^{3}	PD	MEH-PPV + C60, P3OT	Early organic photodiode
30	1996	400–650	60%				PD	MEH-PPV + CdS(Se) quantum dots	Early polymer–quantum-dot–nanocomposite photodiode
31	2000	500–700	75%		10^{12}	4×10^{8}	PD	CuPC/PTCBI	Ultrafast
32	2005	400–700	0.2%		10^{8}	5×10^{4}	PD	CdSe quantum dots	Early quantum-dot photodiode
33	2006	Vis–1300	2700 A W^{-1}	2×10^{13}	5×10^{13}	2×10^{1}	PC	PbS quantum dots	Record sensitivity; pure quantum-dot device
34	2007	Vis–850	120 A W^{-1}	5×10^{12}	3×10^{13}	2×10^{1}	PC	PbS quantum dots	Visible-only device using ultraconfined dots
35	2007	Vis–3000	4.4 A W^{-1}	3×10^{10}		10^{1}	PC	HgTe quantum dots	Long-wavelength operation
36	2008	350–650	50 A W^{-1}		5×10^{12}		PC	P3HT + PCBM + CdTe quantum dots	Sensitive heterojunction device
37	2008	Vis–850	10 A W^{-1}		1.3×10^{13}	5×10^{1}	PC	PbS quantum dots	High-uniformity device
38	2008	Vis–850	12 A W^{-1}	10^{12}		3×10^{1}	PC	PbS quantum dots	Single-trap time constant
39	2008	Vis–900	20 A W^{-1}	10^{11}		2×10^{1}	PC	Bi$_2$S$_3$ nanocrystals	Pb-free, single time constant
40	2008	370–395	61 A W^{-1}		1.3×10^{15}	10^{0}	PC	ZnO quantum dots	Ultraviolet sensitivity
41	2009	250–930	18 A W^{-1}		1.5×10^{14}	3×10^{1}	PC	PbS quantum dots	Multiexciton generation enhanced
42	2009	Vis–1600	0.2 A W^{-1}	10^{12}		10^{6}	PD	PbS quantum dots	Megahertz response in fully depleted photodiode
43	2009	Vis–1300	51%	2×10^{9}		2×10^{3}	PD	PbS quantum dots + PCBM + P3HT	Integrated into an image array
44	2009	Vis–1450	20%		10^{12} near-infrared 10^{13} visible		PD	PDDTT + PCBM	Long-wavelength polymer photodetector
45	2009	400–600	1.5×10^{-5} A W^{-1}			10^{8}	PC	ZnO-infiltrating CQD films	Ultrafast

Measured D obtained from the combination of measured responsivity and measured noise current spectral density.

†Inferred D* based on the assumption that noise-current spectral density is dominated by shot noise in the dark current. This provides a fundamental upper bound on the D* that may actually be achieved in this device.

BW is bandwidth; PD is photodiode; PC is photoconductor; MEH–PPV is poly[2–methoxy–5–(2′ethyl–hexyloxy)–1,4–phenylene vinylene]; PTCBI is 3,4,9,10 perylenetetracarboxylic bisbenzimidazole; CuPC is copper phthalocyanine; P3HT is poly(3–hexylthiophene); PCBM is phenyl–C61–butyric acid methyl ester; P3OT is poly(3–octyl thiophene); PDDTT is poly(5,7–bis(4–decanyl–2–thienyl)thieno[3,4–*b*]diathiazole–thiophene–2,5).

comparable to their exciton lifetimes: thus, well-passivated CQDs incorporated into densely packed solid-state films do not suffer from an excess of non-radiative recombination such as that assisted by midgap recombination centres[57].

As the absorbance of many materials is in the 10^{4}–10^{5} cm^{-1} range near the absorption onset, reaching only 10^{6} cm^{-1} far above the bandgap, it is of interest to make devices that include light-absorption moieties as thick as micrometres. Typically, doping control in CQD solids has led to devices that are fully depleted only if their thicknesses are 100–200 nm (ref. 49). Most micrometre-thick devices will, in this case, be far from fully depleted, demanding efficient transport through a quasi-neutral layer. In this case, the
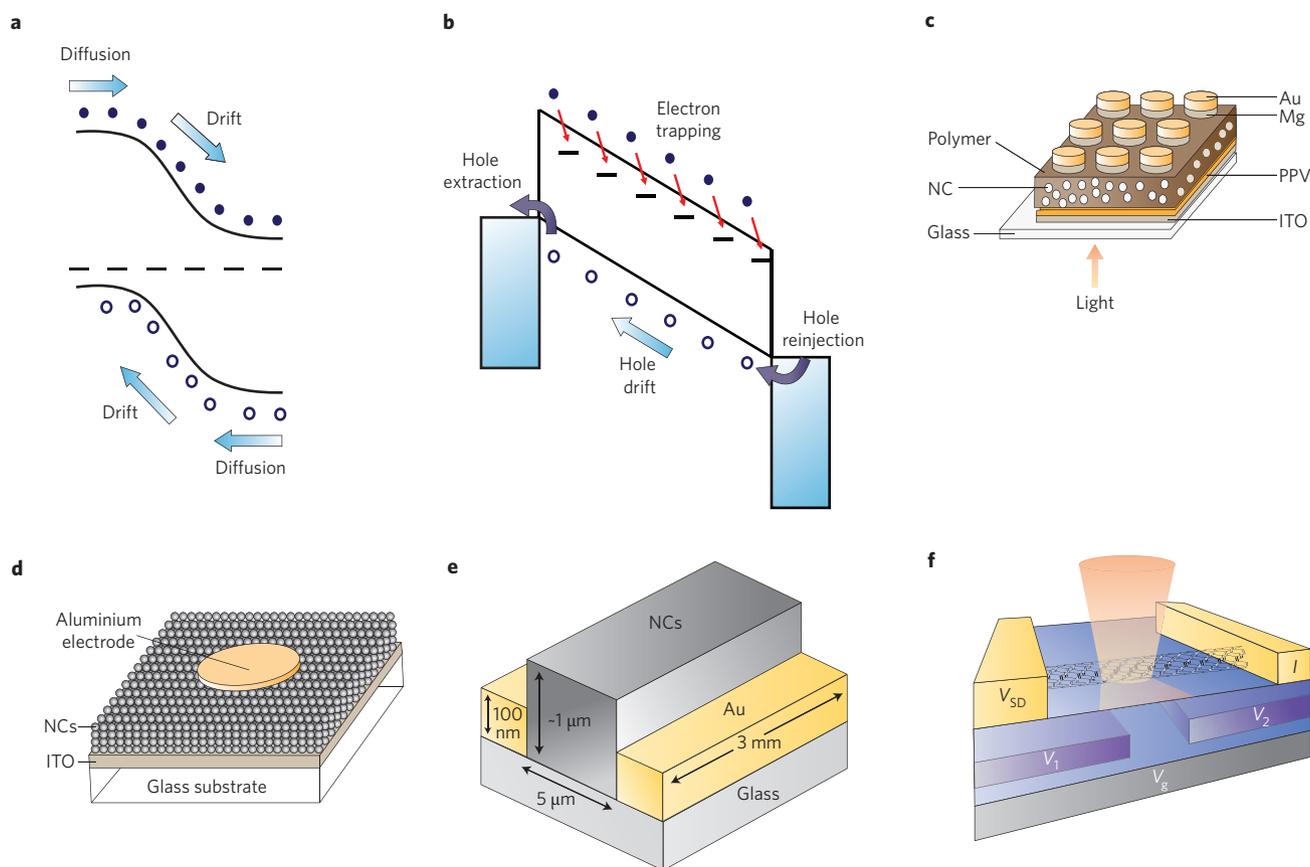
Figure 1 | Photodiodes and photoconductors: charge-separation mechanisms, device structures and configurations. a, Drift and diffusion of both electrons and holes are exploited in photodiodes, in which electron–hole pairs are separated by the action of a built-in electric field represented by the spatial bending of the bands. On light absorption, the energy of the photon is transferred to an electron (filled circles) in the semiconductor, elevating it to the conduction band (upper black line) and leaving behind a hole (open circles) in the valence band (lower black line). This spatial band diagram depicts the junction between a p-type (hole-rich, left side) and n-type (electron-rich, right side) semiconductor near equilibrium. In this p–n junction diode, the dashed line represents the Fermi level. **b**, In a photoconductor, one type of carrier is trapped while the other circulates under the influence of an electric field (electrons are trapped in this depiction). Red arrows depict the capture of electrons from the conduction band into associated trap states. If the hole lifetime exceeds the time it takes for the hole to transit the device, then the long lifetime of the trapped electrons ensures that holes can circulate through an external circuit many times, resulting in gain. **c**, Bulk-heterojunction photodiodes made from a polymer–nanocrystal (NC) composite exploit charge separation across the interface between the polymer matrix and the nanoparticles, and rely on differences in work function between the top and bottom contacts. PPV is poly–phenylene vinylene. **d**, Pure CQD photodiodes consist of a single phase of a quantum-dot thin film across which electrical contacts having different work functions — Fermi levels that are offset from one another before the materials are brought into equilibrium — result in the establishment of a depletion region and built-in field in the CQD film **e**, Lateral photoconductors employ coplanar electrodes coated with a continuous film of nanocrystals. The realization of these devices is greatly simplified by the simple spin casting of a quantum dot (that is, a nanocrystal) film atop electrodes prefabricated on a substrate. The current flow direction is primarily within the horizontal plane. The distance photocarriers must travel — and thus their transit time, relevant to gain — is determined by the contact separation (5 μm in this example). Total current flow is determined by the length of the contacted region (3 mm in the figure) and the height of the film (1 μm in this example). **f**, The conductance of this lateral three-terminal photodetector can be modulated by electrical and/or optical fields (shown in red). The channel in this device is a carbon nanotube. The localized gates V_1, V_2 and the global back gate V_g achieve selective electrostatic doping along the SWNT. V_{SD} is the source-drain voltage. Figures reproduced with permission: **d**, © 2008 OSA; **e**, © 2006 NPG; © 2009 AAAS.

mechanism of minority carrier diffusion will be relied on to convey carriers to the edge of the depletion region to benefit from electron–hole pair separation and extraction.

The diffusion lengths of excitons in organic semiconductors have been found, in a wide variety of materials, to be rather short, lying in the 5–20 nm range[58]. Fortunately, in certain CQD solids, minority diffusion lengths in excess of 100 nm, and reaching as high as 200 nm, have been observed[42,53]. It is believed that, in these studies, the use of very short, conjugated organic linkers — in this case, benzenedithiol — facilitated interdot transport, and the thiol end functional group ensured passivation. Minority electron mobilities of 10^{-3} cm^2 V s^{-1} combined with an absence of midgap traps[57], thus extended diffusion lengths into to these very attractive length-scales

for solution-cast direct-gap optoelectronic materials. There is now widespread evidence that much higher mobilities of 10^{-1} cm^2 V s^{-1} and greater may be achieved in CQD films[21]; once these are combined with efficient passivation and excellent film morphology, considerable further device improvements are in reach.

One result in Table 2 stands out for its combination of excellent sensitivity ($D^* = 10^{12}$ Jones) and high bandwidth in the megahertz range[42]. This high, directly measured D^* is all the more remarkable because of the small bandgap of the device, which provided sensitivity out to 1.6 μm. This is the wavelength of interest for night-time imaging, allowing images to be collected using only the sky's own nightglow[59]. High sensitivity was achieved by means of the joint optimization of electron and hole transport, leading to high

quantum efficiencies, as well as control over film morphology and defect passivation, which maximized the shunt resistance and minimized dark current. The megahertz temporal response was achieved through the realization of a fully depleted device, and this bandwidth further confirms that carriers are extracted through drift in these devices on the submicrosecond timescale.

Photoconductor mechanisms and performance

Photoconductors (Fig. 1b) conduct a single carrier type, and so are unipolar, whereas photodiodes extract carriers of each type. Following illumination, the conductance of photoconductors increases for a duration known as the persistence time. The difference between light versus dark conductance indicates the light level. If the persistence time exceeds the transit time of the flowing carrier through the device, many charges worth of current may be integrated for each photon absorbed. The persistence is determined by the electron–hole pair recombination time, and this is prolonged with the aid of traps[33,36,38,39,41,60,61] (Fig. 2). These traps serve to both delay band-to-band recombination and to impede the extraction of the trapped carrier, a condition necessary for photoconductive gain. The physical mechanisms underlying photoconduction have been of interest in bulk materials since early on in the history of semiconductors[62,63].

The first solution-cast optoelectronic device to outperform its epitaxial counterparts was a photoconductive photodetector reported in 2006 (ref. 33) (Fig. 1e). A key insight leading to this advance was the realization that excess noise could accumulate along the transport path if the interfaces between the nanoparticles making up the semiconductor film were randomly time varying. This multiplicative noise, also known as transport noise, was obviated through a processing strategy in which pure (trap-free) CQD films were first realized; only when the electrical connections between adjacent nanoparticles were forged were the remaining exposed surfaces of the nanoparticles decorated with sensitizing centres (Fig. 2a). In this way, carrier transport along the path of conduction was not modulated by fluctuating barriers.

Many advances in solution-cast photoconductor performance have since been reported. For example, PbS nanoparticles with a diameter of less than 3 nm can have a bandgap that is three times that of bulk PbS, and the resulting strong quantum confinement can be exploited to achieve high-detectivity visible-wavelength light sensing[34]. The quantum size effect affords wide spectral tunability within a single materials system and processing architecture, enabling multispectral detectors that monolithically integrate pixels that are sensitive in the visible, near infrared, and short-wavelength infrared.

Building on a long history of studies of bulk PbS photoconduction[64], recent reports have determined the chemical origins of traps having different energies, and different lifetimes, as a function of chemical species and nanoparticle size and preparation. This enabled the implementation of a single lifetime for trap states, resulting in video-frame-rate-compatible photoconductor behaviour[38]. The latter, in combination with the abundance of surface traps stemming from the high surface-to-volume ratio offered by the nanostructured materials, has led to a dynamic range in the region of 150 dB (ref. 34), well exceeding the requirements of the most demanding imaging applications.

The use of pairs of materials that form charge-separating heterojunctions has been advanced as a promising alternative to surface functionalization for trap engineering. Polymer–nanocrystal pairings have previously been identified, often for applications in photovoltaics, that produce a type-II (charge-separating) junction between quantum dots[60,65] as well as linear and branched nanoparticle architectures[66,67]. An organic material has been employed to provide the phase for carrier transport in a photoconductor, whereas sensitization (trapping) was provided by CQDs incorporated into the mixture having a type-II band alignment relative to the organic component
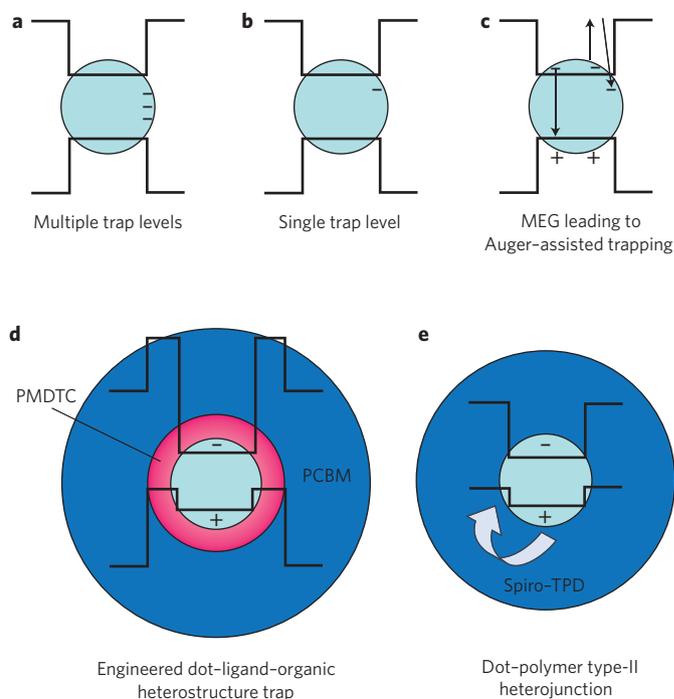

Multiple trap levels Single trap level MEG leading to Auger–assisted trapping

Engineered dot–ligand–organic heterostructure trap

Dot–polymer type-II heterojunction

Figure 2 | Trap engineering in photoconductors. Traps extend the lifetime of non-circulating carriers (Fig. 1b), thereby increasing gain. **a**–**e**, The central light-blue circles represent the CQD. The energy axis is represented in the vertical dimension, the spatial dimension through the horizontal axes. The spatial profile of the valence band edge is the lower solid line, whereas the spatial profile of the conduction band edge is the upper solid line **a**, Multiple sensitizing agents — such as native sulphides, sulphates, and sulphoxides on nanoparticle surfaces — generally result in multiple trap-state lifetimes and a multi-time-constant temporal response[33]. In general, photodetectors and image sensors require a single time constant to achieve a bandwidth that is independent of signal level and substantially linear response. **b**, Traps on nanoparticle surfaces of a single chemical species, and thus a single lifetime, have been implemented through advances in process engineering. A single class of chemical species, such as sulphites, produces a single temporal component in the photodetector's response. These photodetectors offer speeds of response compatible with video-frame-rate imaging[38,39]. **c**, MEG, leading to enhanced Auger recombination in quantum dots in the simultaneous presence of at least two excitons, enhances the rate of capture to traps in one recent report[41]. **d**, Heterostructures, such as those between quantum dots and polymers (here, phenyl–*N*–methyldithiocarbamate (PMDTC) in pink and phenyl–C61–butyric acid methyl ester (PCBM) in dark blue), enable another form of trap-state engineering. In this example, the PMDTC ligand offers a potential barrier for electrons, keeping them confined to the quantum dot, but this same ligand serves as a hole acceptor, providing for spatial separation of photogenerated charges. Quantum size effect tunability within at least one phase can allow band offsets to be tuned[36,60]. **e**, Another recent innovation includes the implementation of devices in which separate paths are provided for electrons and holes. In this example, electrons are confined to the quantum dot, and holes rapidly captured to the N,N'–Bis(3–methylphenyl)–N,N'–bis–(phenyl)–9,9–spiro–bifluorene (spiro-TPD, in dark blue) organic semiconductor. Keeping these phases separated, and contacting each in turn, provided separate paths for the transport of carriers separated across the quantum dot/organic junction[61].

(Fig. 1c)[36]. Quantum-size-effect tuning of not only bandgap, but also band offset, thus offers a complementary path to tuning the energy depth of trap centres in photoconductors based on solution-cast materials (Fig. 2d). Control over surface passivation and the packing
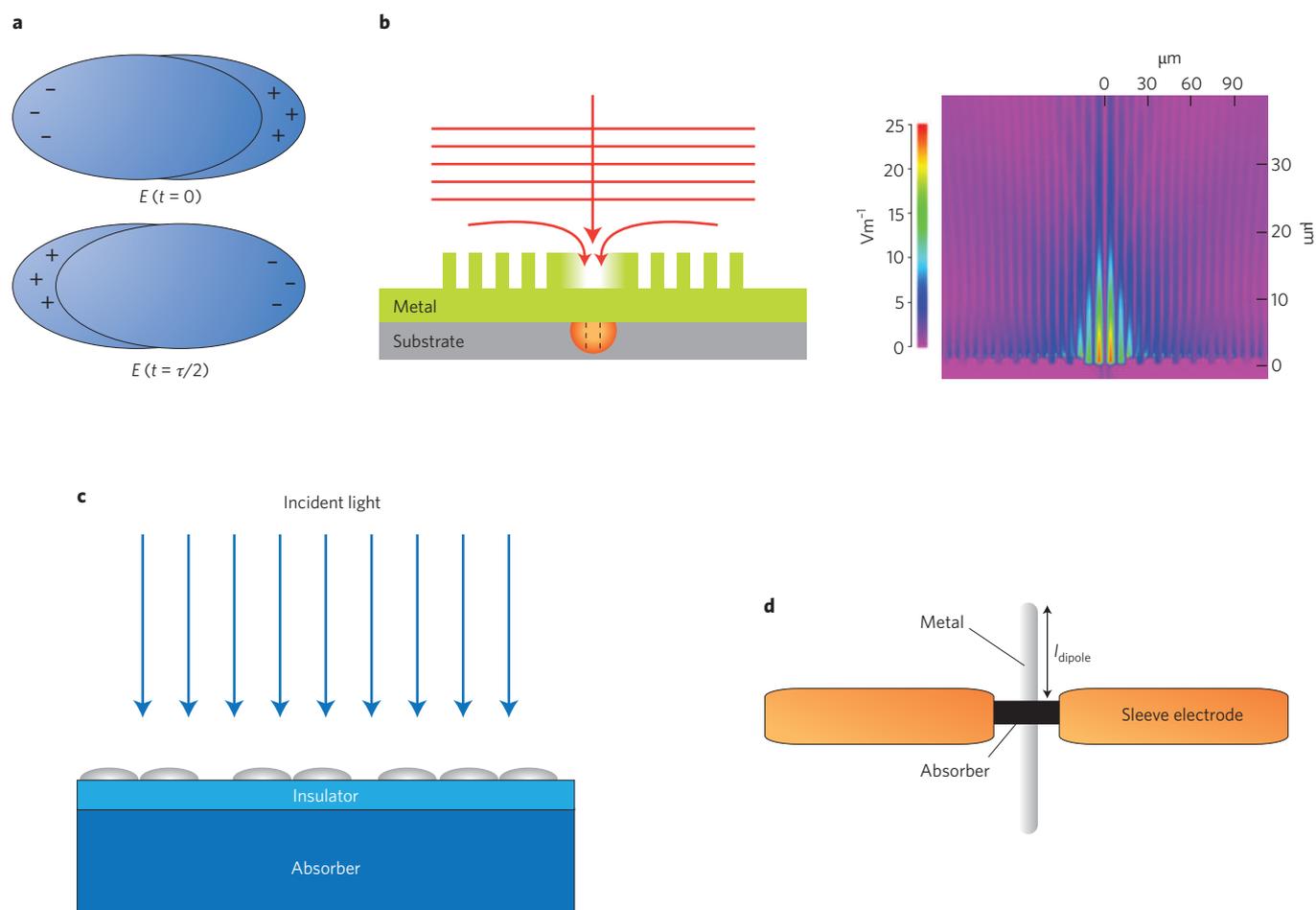
Figure 3 | Plasmonics for enhanced photodetection. Surface plasmon polaritons are collective oscillations of free electrons at the boundary of a metal and a non-conducting dielectric or semiconductor material[88]. **a**, An external electromagnetic field shifts free conduction electrons with respect to the centre of a metal nanoparticle. A resonance follows from the resulting restoring field[89]. **b**, In one approach to plasmonic enhancement of light absorption, photons are localized to a nanoscale slit filled with light-absorbing material. Light is concentrated from the large incidence area into the smaller light-absorber area (shown as an orange semicircle) through the use of SPPs into which coupling is achieved by means of periodic grooves in the metal. The graph on the right shows the amplitude of the normal component of the electric field for a 10-period circular antenna. Field enhancement is observed in the vicinity of the central groove as a result of the wave-guided SPP modes along the periodically grooved metallic plasmon guide[90]. **c**, A sensor achieves enhanced absorption through scattering into a lightly absorbing medium through the use of nanoscale metallic nanoparticles or islands[91]. In this example, ellipsoidal silver nanoparticles of ~16 nm diameter lie in the plane on top of an insulator. The silver nanoparticles produce increased optical interaction, and thus a plasmonic enhancement, of light absorption within the semiconductor beneath. **d**, View from the top of a nanophotonic analogue of an antenna, wherein a metal dipole of length $2l_{dipole}$ enhances light coupling. Light is incident from the top, that is, out of the plane of the figure, into an ultrasmall-volume light absorber electrically contacted by two metal sleeve electrodes[92]. The dipole antenna of length l_{dipole} collects light from a larger area and concentrates it into the small subwavelength region of Ge. Figure reproduced with permission: **b**, © 2008 OSA.

of films through short, suitably functionalized organic ligands was a crucial element of engineering in these materials. An innovative ligand strategy provided a desirable combination of colloidal stability, carrier transport, and passivation of the nanoparticle surface.

Carrier multiplication and prospects

Conventionally, both photodiodes and photoconductors seek to produce a maximum signal following the generation of, at most, one electron–hole pair per photon. A further, multiplicative, path to enhanced signal generation arises if numerous photocarriers can be generated for every photon. Carrier multiplication, known in the CQD literature as multiexciton generation (MEG)[68], offers this possibility. Carrier multiplication has previously been observed in bulk photodetectors[69], and MEG has been observed in CQDs for more than half a decade[24]; however, its benefits were only recently observed in the photocurrent of an operating CQD device[41,70,71]. Furthermore, the energetic threshold and yield of MEG have been

the subject of debate, with variations arising as a function of spectroscopic technique and sample preparation[72–74]. Recently, a photoconductive photodetector employing CQDs[41] was observed to exhibit spectrally invariant internal photoconductive gain until the onset of MEG at a photon energy equal to slightly less than three times the quantum-confined bandgap; at higher photon energies, a steep rise in internal gain was observed. Such phenomena had previously been sought, but not seen, in photodiodes based on similar quantum-dot materials[55]. Although the Auger recombination process in the presence of several excitons rapidly leads to annihilation of primary photoexcitations in photodiodes, the same process leads to efficient ionization[72] and capture to the traps that sensitize photoconductors[75]. Direct ionization of excited photocarriers prior to MEG could, in principle, also be expected to occur; however, a series of control experiments[41] investigating the size-effect and trap-depth dependence of the internal gain spectrum suggest that direct ionization does not play a leading role in photoresponse. Taken in

combination, these findings indicate that the carrier multiplication process occurs more rapidly than both intersubband relaxation and direct capture of excited photocarriers to traps.

The generation of many electron–hole pairs per photon has also been reported in single-walled nanotube photodiodes[76] (Fig. 1f). Devices consisted of an electrostatically doped nanotube in a split-gate field-effect transistor architecture: a p–n junction was formed along the nanotube[77] and the photocurrent response at reverse bias was monitored as a function of the photon energy. Photocurrent was found to increase on illumination by photons having energies greater than twice the bandgap energy, and to exhibit a step-wise dependence on the applied bias with a period equal to the bandgap of the nanotube. The photocurrent increase was ascribed to multiple electron–hole generation, an effect that may be favoured in nanotubes by virtue of a low Fermi velocity combined with a low dielectric constant. Although the reported effect was observed only below 150 K, the approach indicates the potential for nanowire-based photodetectors[78] that provide light detection in the near-infrared and visible parts of the spectrum.

Progress in organic and alternative inorganic materials

Purely organic photodiodes[29] have, until very recently, been largely limited to the visible wavelength regime by virtue of the energies of the transition between the highest occupied molecular orbital (HOMO) and the lowest unoccupied molecular orbital (LUMO) typically available in these materials[79]. In 2009, however, an organic photodiode was successfully engineered to have a promising combination of spectral response and inferred sensitivity[44]. The extrapolated D^* (based on a best-case assumption that the dark-current noise was bounded by the shot-noise mechanism) exceeded 10^{12} Jones including out to 1,450 nm — dramatically beyond the previous reach of HOMO–LUMO transitions in optoelectronic devices based on organics and polymers[80]. The key to longer-wavelength light absorption was the polymer poly(5,7-*bis*(4-decanyl-2-thienyl)-thieno (3,4-b)diathiazole-thiophene-2,5) (PDDTT; ref. 81). A relatively low-bandgap monomeric repeat unit (~1.6 eV) was arrayed periodically to produce a polymer with 1.1 eV bandgap and considerable absorption all the way out to 1,450 nm.

One potential concern in many CQD studies is the reliance on model systems that employ heavy metals such as Cd or Pb. New optoelectronic nanomaterials that avoid these issues include reports on Ag_2S (ref. 82), Bi_2S_3 (ref. 83), In_2S_3 (ref. 84) and Cu_2S (ref. 85), each of which have seen initial investigation with regard to photodetection.

Device longevity under illumination is another critical issue for commercial application. There are indications that — when nanoparticle surfaces are suitably stabilized using robust inorganic[86] or organic treatments[53] — air stability can be achieved. Also of critical importance is the semiconductor/metal interface, shown to benefit from inclusion of a diffusion-blocking interlayer such as LiF (ref. 87).

Plasmonics for sensitive and fast photodetection

The best solution-processed photodetectors are now approaching the fundamental limits of device sensitivity and speed in the absence of optical concentration[48]. The field of plasmonics[88–92] (Fig. 3), which has seen tremendous advancements[93], offers further potential to concentrate light into small-volume photodetectors, potentially leading to further leaps in photodetector performance.

The free electrons in a metal behave as a gas, or plasma, of free charge carriers. They can be excited to sustain a propagating plasma wave. Surface plasmons are bound to the interface of the plasma and a dielectric[89]. For small metal nanoparticles, an external electromagnetic field can penetrate the nanoparticle and shift the free conduction electrons with respect to the centre of the particle. This produces opposing surface charges on the opposite surfaces of the particles (Fig. 3a) and results in a restoring field. The

coherently shifted electrons of the metal particle, together with the restoring field, constitute an oscillator with a defined resonance. These resonances are typically found in the visible or near infrared in metal nanoparticles.

If excited at resonance, the amplitude of the induced electromagnetic field on a surface plasmon on a metal nanoparticle can exceed the exciting field by more than an order of magnitude. This is known as the near-field enhancement. In the far field, the size dependence of the absorption and scattering cross sections of surface plasmons on a metal nanoparticle offers size-engineerable advantages: the scattering depends on the square of the particle volume, whereas the absorption depends only linearly on the particle volume. Thus, small particles are dominated by absorption, but large particles by scattering.

One of the main concepts in plasmonics that offers significant benefits in photodetection is that light from a wide beam can be coupled efficiently into a narrow aperture in which the detector resides. The area of the beam and the area of the detector need no longer be the same. Instead, functioning like an antenna, a plasmonic lens concentrates light into a much smaller detecting volume. The low dark current, low noise and high speed of the small detector may then be exploited without sacrifice to the absorbing cross-section of the device.

In 2006, Brongersma *et al.* proposed a photodetector design that used plasmonic effects to concentrate light, incident over a wide area, in a narrow slice of light-absorbing semiconductor[90] (Fig. 3b). Light is incident on a device having an areal cross-section perpendicular to the beam that allows full capture of the incident radiation. The device is designed to guide, or concentrate, the light towards a narrow, central light absorber by coupling into surface plasmon polariton (SPP) modes that propagate laterally in the plane.

There are two components to the resultant enhancement in absorbance. The first comes from placing the semiconductor material inside a metal cavity. Compared with a planar slab made of the same absorbing material, the use of this single metal slit provides a tenfold enhancement[94]. The grating is responsible for coupling the incident near-plane-wave into an SPP mode that then guides light towards the slit. Taken together, the lateral coupling and the Fabry–Perot resonance within the slit offer a 250-fold enhancement in absorbance compared with an unenhanced absorber. Similar concepts involving two-dimensional nanostructuring of metals, such as in cylindrical[95,96] and hexagonal arrays[97], offer the added advantage of polarization-independent concentration. Similarly, the power of plasmonics to boost solar-cell performance across the Sun's broad spectrum has been formalized in a set of practical design guidelines[98].

Another ultralow-volume detector was demonstrated based on a Ge absorber and the antenna-style gold metal design[92]. A dipole antenna (Fig. 3d) was used to collect light from a larger area and concentrate it into the small subwavelength region of Ge. Metal sleeves in the perpendicular direction were used to collect the photocurrent from the semiconductor without substantially perturbing the design of the antenna's dipole resonance. In this deliberately highly polarization-dependent device, the ratio of photocurrent produced in the case of the two orthogonal polarizations (one aligned with the dipolar antenna, the other perpendicular to it) was used as proxy for the absorption enhancement owing to the dipole. A 20-fold enhancement was achieved in this manner. The optical-antenna concept has been deployed in purely dielectric structures as well: a nanowire Ge photodetector and its dependence on wavelength and polarization were explored in the framework of leaky resonant modes that allow coupling of optical-wavelength-scale excitations to subwavelength cavities, making up nanoscale photodetector volumes[99].

Much of the work discussed in this review is motivated by the benefits of low-cost, large-area solution processing. To maintain these benefits, it is of interest to exploit plasmonic effects that do not rely on top-down nanoscale patterning. Localized surface plasmon

effects, based on colloidal metal nanoparticles or self-assembled metal islands, offer compatibility with the solution processing. Silicon photodetectors[100] and solar cells[91] with suitably sized metal islands on top of the light-absorbing medium have been shown to provide greater than tenfold enhancements in their absorbance and photocurrents. These results were improved on by the use of an optically thin layer of silicon whose single-pass absorbance in the near infrared was on the order of a few per cent. The enhancement derived from efficient scattering into the weakly absorbing silicon (Fig. 3c) and is a technologically viable alternative to light-trapping approaches based on dielectric scattering.

Of intense interest is the direct electrical detection of SPPs. Plasmonic circuits offer the prospect of conveying signals across electronic chips with speed and greater compactness compared with even highly confining optical waveguides[101], promising to marry components on the electronics lengthscale (that is, sub-100 nm) with the vast information-carrying capacity of the optical channel[102]. One of the key challenges for the field has been the realization of a suitable combination of plasmon sources[103] and detectors. Direct electrical detection of plasmons has been reported[104–106]. In one of the first examples, near-field coupling of a metal nanoparticle to a nanostructured GaAs photodetector was achieved[104]. Near-field electrical detection of plasmons generated by single-plasmon sources has also been shown[107]: a CdSe CQD was optically excited to produce single plasmons that were coupled into a plasmonic metal waveguide. The resultant SPP propagated over many micrometres and was detected through coupling of the near field of the metallic waveguide to a Ge nanowire photodetector resulting in the generation of electron–hole pairs that were collected in the electrodes contacting the Ge nanowire. By exploiting photoconductive gain in the Ge nanowire, a detector responsivity of 50 electrons per plasmon was achieved. Ultimately the field offers an attractive union of semiconductor plasmon sources, such as CQDs, acting in the role of active sources and detectors, integrated with metal nanoparticles acting as plasmonic waveguides, the combination leading towards all-solution-processed plasmonic nanocircuits.

Advances in materials chemistry offer excellent possibilities in the direct coupling — at the time of synthesis — of plasmonic source and detection materials with metal nanoparticles. Talapin *et al.* have reported[108] an all-solution-phase approach to such a coupled synthesis and deposition, in which Au nanoparticles were first synthesized, after which PbS was overgrown around the metal nanoparticle seeds. A multicomponent material was thus formed consisting of a core–shell Au–PbS heterostructure. The final nanocrystals were then isolated to form a stable colloid. An absorbance enhancement of 28% was reported compared with an uncoupled mixture of Au nanoparticles and PbS quantum dots.

Conventional plasmon-enhanced photodetection consists of a two-component materials system: metal nanoparticles to induce the plasmon effects that will in turn be coupled to a semiconductor nanoparticle with the appropriate bandgap to form electron–hole pairs. Recent advances seek to unite plasmonic effects with the optical-to-electronic transduction mechanism[109], including by means of direct absorption in the metal nanoparticle phase itself[110].

Clearly, plasmonic effects hold great promise in enhancing photodetector performance. For this promise to be fully realized, it is necessary for absolute, rather than relative, enhancements in photocurrent — and ultimately photodetector performance — to be demonstrated experimentally. Achieving high bandwidth in solution-processed CQD devices has so far relied on using fully depleted, hence thin and incompletely absorptive, amounts of active material. Plasmonics offers the prospect of complete absorbance combined with speed — prospectively leading to an improvement in gain-bandwidth product on the order of the plasmonic absorbance enhancement, thus exceeding an order of magnitude. The sensitivity of detectors, as quantified by figures such as D^*, may be similarly enhanced by concentrating light waves into a dramatically reduced volume of detecting material.

Conclusions

Solution-processed nanostructured light sensors offer many advantages for imaging and photodetection applications. The convenient integration of light-sensing materials with a variety of substrates enables the separate optimization of distinct device functions. For example, silicon electronics, ideally suited to high-volume manufacture, can provide low-noise read-out, along with a comprehensive array of analogue and digital functions. A nanostructured light-sensing layer can meanwhile be designed to optimize fill factor, absorption spectrum, optical density, and crosstalk. The ever-growing proficiency in manipulating materials at the nanoscale, on quantum- and plasmonic-length scales, will allow an unprecedented degree of customization and optimization in future generations of light-sensing arrays.

Corrected online: 4 June 2010

References

1. Bartels, R. A. *et al.* Generation of spatially coherent light at extreme ultraviolet wavelengths. *Science* **297,** 376–378 (2002).
2. Zeskind, B. J. *et al.* Nucleic acid and protein mass mapping by live-cell deep-ultraviolet microscopy. *Nature Methods* **4,** 567–569 (2007).
3. Dawes, D. G. & Turner, D. Some like it hot. *Photonics Spectra* **42,** 72–74 (2008).
4. Formisano, V., Atreya, S., Encrenaz, T., Ignatiev, N. & Giuranna, M. Detection of methane in the atmosphere of Mars. *Science* **306,** 1758–1761 (2004).
5. Fossum, E. R. CMOS image sensors: electronic camera-on-a-chip. *IEEE Trans. Electron. Dev.* **44,** 1689–1698 (1997).
6. Les, C. B. Image sensor market: Changing, but moving upward. *Photonics Spectra* **43,** 27–28 (2009).
7. El Gamal, A. & Eltoukhy, H. CMOS image sensors. *IEEE Circuits Devices Mag.* **21,** 6–20 (2005).
8. Herzinger, C. M., Johs, B., McGahan, W. A., Woollam, J. A. & Paulson, W. Ellipsometric determination of optical constants for silicon and thermally grown silicon dioxide via a multi-sample, multi-wavelength, multi-angle investigation. *J. Appl. Phys.* **83,** 3323–3336 (1998).
9. Minoglou, K. *et al.* Reduction of electrical crosstalk in hybrid backside illuminated CMOS imagers using deep trench isolation. *2008 IEEE Int. Interconnect Technol. Conf.* 129–131 (2008).
10. Prydderch, M. *et al.* A large area CMOS monolithic active pixel sensor for extreme ultra violet spectroscopy and imaging. *Proc. SPIE* **5301,** 175–185 (2004).
11. Sosnowski, L., Starkiewicz, J. & Simpson, O. Lead sulphide photoconductive cells. *Nature* **159,** 818–819 (1947).
12. Espevik, S., Wu, C. H. & Bube, R. H. Mechanism of photoconductivity in chemically deposited lead sulfide layers. *J. Appl. Phys.* **42,** 3513–3529 (1971).
13. Kanno, T. *et al.* Uncooled infrared focal plane array having 128 x 128 thermopile detector elements. *Proc. SPIE* **2269,** 450–459 (1994).
14. Nausieda, I. *et al.* An organic active-matrix imager. *IEEE Trans. Electron Devices* **55,** 527–532 (2008).
15. Shchukin, V. A. & Bimberg, D. Spontaneous ordering of nanostructures on crystal surfaces. *Rev. Mod. Phys.* **71,** 1125–1171 (1999).
16. Murray, C. B., Norris, D. J. & Bawendi, M. G. Synthesis and characterization of nearly monodisperse CdE (E = S, Se, Te) semiconductor nanocrystallites. *J. Am. Chem. Soc.* **115,** 8706–8715 (1993).
17. Sun, Y. & Xia, Y. Shape-controlled synthesis of gold and silver nanoparticles. *Science* **298,** 2176–2179 (2002).
18. Brus, L. Electronic wave functions in semiconductor clusters: Experiment and theory. *J. Phys. Chem.* **90,** 2555–2560 (1986).
19. Kelly, K. L., Coronado, E., Zhao, L. L. & Schatz, G. C. The optical properties of metal nanoparticles: The influence of size, shape, and dielectric environment. *J. Phys. Chem. B* **107,** 668–677 (2003).
20. Mi, Z., Yang, J., Bhattacharya, P., Qin, G. & Ma, Z. High-performance quantum dot lasers and integrated optoelectronics on Si. *Proc. IEEE* **97,** 1239–1249 (2009).
21. Talapin, D. V. & Murray, C. B. PbSe nanocrystal solids for n- and p-channel thin film field-effect transistors. *Science* **310,** 86–89 (2005).
22. Yu, D., Wang, C., Wehrenberg, B. L. & Guyot-Sionnest, P. Variable range hopping conduction in semiconductor nanocrystal solids. *Phys. Rev. Lett.* **92,** 216802 (2004).
23. Pandey, A. & Guyot-Sionnest, P. Slow electron cooling in colloidal quantum dots. *Science* **322,** 929–932 (2008).

24. Schaller, R. D. & Klimov, V. I. High efficiency carrier multiplication in PbSe nanocrystals: Implications for solar energy conversion. *Phys. Rev. Lett.* **92,** 186601 (2004).

25. Klimov, V. I. *et al.* Optical gain and stimulated emission in nanocrystal quantum dots. *Science* **290,** 314–317 (2000).

26. Klimov, V. I., Mikhailovsky, A. A., McBranch, D. W., Leatherdale, C. A. & Bawendi, M. G. Quantization of multiparticle Auger rates in semiconductor quantum dots. *Science* **287,** 1011–1014 (2000).

27. Klimov, V. I. Optical nonlinearities and ultrafast carrier dynamics in semiconductor nanocrystals. *J. Phys. Chem. B* **104,** 6112–6123 (2000).

28. Ellingson, R. J. *et al.* Highly efficient multiple exciton generation in colloidal PbSe and PbS quantum dots. *Nano Lett.* **5,** 865–871 (2005).

29. Yu, G., Pakbaz, K. & Heeger, A. J. Semiconducting polymer diodes: Large size, low cost photodetectors with excellent visible-ultraviolet sensitivity. *Appl. Phys. Lett.* **64,** 3422–3424 (1994).

30. Greenham, N. C., Peng, X. & Alivisatos, A. P. Charge separation and transport in conjugated-polymer/semiconductor-nanocrystal composites studied by photoluminescence quenching and photoconductivity. *Phys. Rev. B* **54,** 17628–17637 (1996).

31. Peumans, P., Bulovic, V. & Forrest, S. R. Efficient, high-bandwidth organic multilayer photodetectors. *Appl. Phys. Lett.* **76,** 3855–3857 (2000).

32. Oertel, D. C., Bawendi, M. G., Arango, A. C. & Bulovic, V. Photodetectors based on treated CdSe quantum-dot films. *Appl. Phys. Lett.* **87,** 213505 (2005).

33. Konstantatos, G. *et al.* Ultrasensitive solution-cast quantum dot photodetectors. *Nature* **442,** 180–183 (2006).

34. Konstantatos, G., Clifford, J., Levina, L. & Sargent, E. H. Sensitive solution-processed visible-wavelength photodetectors. *Nature Photon.* **1,** 531–534 (2007).

35. Boberl, M., Kovalenko, M. V., Gamerith, S., List, E. J. W. & Heiss, W. Inkjet-printed nanocrystal photodetectors operating up to 3 um wavelengths. *Adv. Mater.* **19,** 3574–3578 (2007).

36. Chen, H. Y., Lo, M. K. F., Yang, G., Monbouquette, H. G. & Yang, Y. Nanoparticle-assisted high photoconductive gain in composites of polymer and fullerene. *Nat. Nanotech.* **3,** 543–547 (2008).

37. Hinds, S. *et al.* Smooth-morphology ultrasensitive solution-processed photodetectors. *Adv. Mater.* **20,** 4398–4402 (2008).

38. Konstantatos, G., Levina, L., Fischer, A. & Sargent, E. H. Engineering the temporal response of photoconductive photodetectors via selective introduction of surface trap states. *Nano Lett.* **8,** 1446–1450 (2008).

39. Konstantatos, G., Levina, L., Tang, J. & Sargent, E. H. Sensitive solution-processed Bi2S3 nanocrystalline photodetectors. *Nano Lett.* **8,** 4002–4006 (2008).

40. Jin, Y., Wang, J., Sun, B., Blakesley, J. C. & Greenham, N. C. Solution-processed ultraviolet photodetectors based on colloidal ZnO nanoparticles. *Nano Lett.* **8,** 1649–1653 (2008).

41. Sukhovatkin, V., Hinds, S., Brzozowski, L. & Sargent, E. H. Colloidal quantum-dot photodetectors exploiting multiexciton generation. *Science* **324,** 1542–1544 (2009).

42. Clifford, J. P. *et al.* Fast, sensitive and spectrally tuneable colloidal-quantum-dot photodetectors. *Nature Nanotech.* **4,** 40–44 (2009).

43. Rauch, T. *et al.* Near-infrared imaging with quantum-dot-sensitized organic photodiodes. *Nature Photon.* **3,** 332–336 (2009).

44. Gong, X. *et al.* High-detectivity polymer photodetectors with spectral response from 300 nm to 1450 nm. *Science* **325,** 1665–1667 (2009).

45. Pourret, A., Guyot-Sionnest, P. & Elam, J. W. Atomic layer deposition of ZnO in quantum dot thin films. *Adv. Mater.* **21,** 232–235 (2009).

46. Petritz, R. L. Theory of photoconductivity in semiconductor films. *Phys. Rev.* **104,** 1508–1516 (1956).

47. Cova, S., Ghioni, M., Lacaita, A., Samori, C. & Zappa, F. Avalanche photodiodes and quenching circuits for single-photon detection. *Appl. Opt.* **35,** 1956–1976 (1996).

48. Piotrowski, J. & Gawron, W. Ultimate performance of infrared photodetectors and figure of merit of detector material. *Infrared Phys. Technol.* **38,** 63–68 (1997).

49. Johnston, K. W. *et al.* Efficient Schottky-quantum-dot photovoltaics: The roles of depletion, drift, and diffusion. *Appl. Phys. Lett.* **92,** 122111 (2008).

50. Clark, S. W., Harbold, J. M. & Wise, F. W. Resonant energy transfer in PbS quantum dots. *J. Phys. Chem. C* **111,** 7302–7305 (2007).

51. Klem, E. J. D., MacNeil, D. D., Cyr, P. W., Levina, L. & Sargent, E. H. Efficient solution-processed infrared photovoltaic cells: Planarized all-inorganic bulk heterojunction devices via inter-quantum-dot bridging during growth from solution. *Appl. Phys. Lett.* **90,** 183113 (2007).

52. Johnston, K. W. *et al.* Schottky-quantum dot photovoltaics for efficient infrared power conversion. *Appl. Phys. Lett.* **92,** 151115 (2008).

53. Koleilat, G. I. *et al.* Efficient, stable infrared photovoltaics based on solution-cast colloidal quantum dots. *ACS Nano* **2,** 833–840 (2008).

54. Luther, J. M. *et al.* Schottky solar cells based on colloidal nanocrystal films. *Nano Lett.* **8,** 3488–3492 (2008).

55. Law, M. *et al.* Determining the internal quantum efficiency of PbSe nanocrystal solar cells with the aid of an optical model. *Nano Lett.* **8,** 3904–3910 (2008).

56. Ma, W., Luther, J. M., Zheng, H., Wu, Y. & Alivisatos, A. P. Photovoltaic devices employing ternary PbSxSe1-x nanocrystals. *Nano Lett.* **9,** 1699–1703 (2009).

57. Barkhouse, D. A. R., Pattantyus-Abraham, A. G., Levina, L. & Sargent, E. H. Thiols passivate recombination centers in colloidal quantum dots leading to enhanced photovoltaic device efficiency. *ACS Nano* **2,** 2356–2362 (2008).

58. Coakley, K. M. & McGehee, M. D. Conjugated polymer photovoltaic cells. *Chem. Mater.* **16,** 4533–4542 (2004).

59. Ettenberg, M. A little night vision. *Advanced Imaging* **20,** 29–32 (2005).

60. McDonald, S. A. *et al.* Solution-processed PbS quantum dot infrared photodetectors and photovoltaics. *Nature Mater.* **4,** 138–142 (2005).

61. Osedach, T. P. *et al.* Lateral heterojunction photodetector consisting of molecular organic and colloidal quantum dot thin films. *Appl. Phys. Lett.* **94,** 043307 (2009).

62. Bube, R. *Photoconductivity of Solids* (Wiley, 1960).

63. Rose, A. *Concepts in Photoconductivity and Allied Problems* 168 (Wiley, 1963).

64. Mahlman, G. W. Photoconductivity of lead sulfide films. *Phys. Rev.* **103,** 1619–1630 (1956).

65. Greenham, N. C., Peng, X. & Alivisatos, A. P. Charge separation and transport in conjugated polymer/cadmium selenide nanocrystal composites studied by photoluminescence quenching and photoconductivity. *Synth. Met.* **84,** 545–546 (1997).

66. Huynh, W. U., Dittmer, J. J. & Alivisatos, A. P. Hybrid nanorod-polymer solar cells. *Science* **295,** 2425–2427 (2002).

67. Milliron, D. *et al.* Colloidal nanocrystal heterostructures with linear and branched topology. *Nature* **430,** 190–195 (2004).

68. Nozik, A. J. Multiple exciton generation in semiconductor quantum dots. *Chem. Phys. Lett.* **457,** 3–11 (2008).

69. Smith, A. & Dutton, D. Behavior of Lead Sulfide Photocells in the Ultraviolet. *J. Opt. Soc. Am.* **48,** 1007–1009 (1958).

70. Kim, S. J., Kim, W. J., Sahoo, Y., Cartwright, A. N. & Prasad, P. N. Multiple exciton generation and electrical extraction from a PbSe quantum dot photoconductor. *Appl. Phys. Lett.* **92,** 031107 (2008).

71. Kim, S. J., Kim, W. J., Cartwright, A. N. & Prasad, P. N. Carrier multiplication in a PbSe nanocrystal and P3HT/PCBM tandem cell. *Appl. Phys. Lett.* **92,** 191107 (2008).

72. McGuire, J. A., Joo, J., Pietryga, J. M., Schaller, R. D. & Klimov, V. I. New aspects of carrier multiplication in semiconductor nanocrystals. *Acc. Chem. Res.* **41,** 1810–1819 (2008).

73. Nair, G., Geyer, S. M., Chang, L. Y. & Bawendi, M. G. Carrier multiplication yields in PbS and PbSe nanocrystals measured by transient photoluminescence. *Phys. Rev. B* **78,** 125325 (2008).

74. Pijpers, J. J. H. *et al.* Assessment of carrier-multiplication efficiency in bulk PbSe and PbS. *Nature Phys.* **5,** 811–814 (2009).

75. Nozik, A. J. Making the most of photons. *Nature Nanotech.* **4,** 548–549 (2009).

76. Gabor, N. M., Zhong, Z., Bosnick, K., Park, J. & McEuen, P. L. Extremely efficient multiple electron-hole pair generation in carbon nanotube photodiodes. *Science* **325,** 1367–1371 (2009).

77. Lee, J. U., Gipp, P. P. & Heller, C. M. Carbon nanotube p-n junction diodes. *Appl. Phys. Lett.* **85,** 145–147 (2004).

78. Hayden, O., Agarwal, R. & Lieber, C. M. Nanoscale avalanche photodiodes for highly sensitive and spatially resolved photon detection. *Nature Mater.* **5,** 352–356 (2006).

79. Peumans, P., Yakimov, A. & Forrest, S. R. Small molecular weight organic thin-film photodetectors and solar cells. *J. Appl. Phys.* **93,** 3693–3723 (2003).

80. Winder, C. & Sariciftci, N. S. Low bandgap polymers for photon harvesting in bulk heterojunction solar cells. *J. Mater. Chem.* **14,** 1077–1086 (2004).

81. Xia, Y. *et al.* Photocurrent response wavelength up to 1.1 um from photovoltaic cells based on narrow-band-gap conjugated polymer and fullerene derivative. *Appl. Phys. Lett.* **89,** 081106 (2006).

82. Wang, D. *et al.* Ultralong single-crystalline Ag2S nanowires: Promising candidates for photoswitches and room-temperature oxygen sensors. *Adv. Mater.* **20,** 2628–2632 (2008).

83. Konstantatos, G., Levina, L., Tang, J. & Sargent, E. H. Sensitive solution-processed Bi2S3 nanocrystalline photodetectors. *Nano Lett.* **8,** 4002–4006 (2008).

84. Tang, J. *et al.* Heavy-metal-free solution-processed nanoparticle-based photodetectors: doping of intrinsic vacancies enables engineering of sensitivity and speed. *ACS Nano* **3,** 331–338 (2009).

85. Wu, Y., Wadia, C., Ma, W., Sadtler, B. & Alivisatos, A. P. Synthesis and photovoltaic application of copper(1) sulfide nanocrystals. *Nano Lett.* **8,** 2345–2350 (2008).

86. Gur, I., Fromer, N. A., Geier, M. L. & Alivisatos, A. P. Materials science: Air-stable all-inorganic nanocrystal solar cells processed from solution. *Science* **310,** 462–465 (2005).

87. Tang, J. *et al.* Schottky quantum dot solar cells stable in air under solar illumination. *Adv. Mater.* **22,** 1398–1402 (2010).

88. Ozbay, E. Plasmonics: Merging photonics and electronics at nanoscale dimensions. *Science* **311,** 189–193 (2006).
89. Maier, S. A. *et al.* Plasmonics - A route to nanoscale optical devices. *Adv. Mater.* **13,** 1501–1505 (2001).
90. Yu, Z., Veronis, G., Fan, S. & Brongersma, M. L. Design of midinfrared photodetectors enhanced by surface plasmons on grating structures. *Appl. Phys. Lett.* **89,** 151116 (2006).
91. Pillai, S., Catchpole, K. R., Trupke, T. & Green, M. A. Surface plasmon enhanced silicon solar cells. *J. Appl. Phys.* **101,** 093105 (2007).
92. Tang, L. *et al.* Nanometre-scale germanium photodetector enhanced by a near-infrared dipole antenna. *Nature Photon.* **2,** 226–229 (2008).
93. Polman, A. Applied physics: Plasmonics applied. *Science* **322,** 868–869 (2008).
94. White, J. S. *et al.* Extraordinary optical absorption through subwavelength slits. *Opt. Lett.* **34,** 686–688 (2009).
95. Bhat, R. D. R., Panoiu, N. C., Brueck, S. R. J. & Osgood Jr, R. M. Enhancing the signal-to-noise ratio of an infrared photodetector with a circular metal grating. *Opt. Express* **16,** 4588–4596 (2008).
96. Ishi, T., Fujikata, J., Marita, K., Baba, T. & Ohashi, K. Si nano-photodiode with a surface plasmon antenna. *Jpn. J. Appl. Phys.* **44,** L364–L366 (2005).
97. Ferry, V. E., Sweatlock, L. A., Pacifici, D. & Atwater, H. A. Plasmonic nanostructure design for efficient light coupling into solar cells. *Nano Lett.* **8,** 4391–4397 (2008).
98. Pala, R. A., White, J., Barnard, E., Liu, J. & Brongersma, M. L. Design of plasmonic thin-film solar cells with broadband absorption enhancements. *Adv. Mater.* **21,** 3504–3509 (2009).
99. Cao, L. *et al.* Engineering light absorption in semiconductor nanowire devices. *Nature Mater.* **8,** 643–647 (2009).
100. Stuart, H. R. & Hall, D. G. Island size effects in nanoparticle-enhanced photodetectors. *Appl. Phys. Lett.* **73,** 3815–3817 (1998).
101. Maier, S. A. The best of both worlds. *Nature Photonics* **2,** 460–461 (2008).
102. Zia, R., Schuller, J. A., Chandran, A. & Brongersma, M. L. Plasmonics: the next chip-scale technology. *Mater. Today* **9,** 20–27 (2006).
103. Noginov, M. A. *et al.* Demonstration of a spaser-based nanolaser. *Nature* **460,** 1110–1112 (2009).
104. De Vlaminck, I., Van Dorpe, P., Lagae, L. & Borghs, G. Local electrical detection of single nanoparticle plasmon resonance. *Nano Lett.* **7,** 703–706 (2007).
105. Neutens, P., Van Dorpe, P., De Vlaminck, I., Lagae, L. & Borghs, G. Electrical detection of confined gap plasmons in metal-insulator-metal waveguides. *Nature Photon.* **3,** 283–286 (2009).
106. Shackleford, J. A., Grote, R., Currie, M., Spanier, J. E. & Nabet, B. Integrated plasmonic lens photodetector. *Appl. Phys. Lett.* **94,** 083501 (2009).
107. Falk, A. L. *et al.* Near-field electrical detection of optical plasmons and single-plasmon sources. *Nature Phys.* **5,** 475–479 (2009).
108. Lee, J. S., Shevchenko, E. V. & Talapin, D. V. Au-PbS core-shell nanocrystals: Plasmonic absorption enhancement and electrical doping via intra-particle charge transfer. *J. Am. Chem. Soc.* **130,** 9673–9675 (2008).
109. Bakr, O. M. *et al.* Silver nanoparticles with broad multiband linear optical absorption. *Angew. Chem. Int. Ed.* **48,** 5921–5926 (2009).
110. Nakanishi, H. *et al.* Photoconductance and inverse photoconductance in films of functionalized metal nanoparticles. *Nature* **460,** 371–375 (2009).

Nanostructured materials for photon detection

Gerasimos Konstantatos and Edward H. Sargent

In the version of this Review originally published online, an error led to Fig. 2c appearing incorrectly; this has now been corrected.